Energy & Environmental Science

ROYAL SOCIETY OF CHEMISTRY

PAPER

View Article Online
View Journal | View Issue

Cite this: *Energy Environ. Sci.*, 2022, **15**, 4710

Generalised predictability in the synthesis of biocarbons as clean energy materials: targeted high performance CO_2 and CH_4 storage†

Ibtisam Alali[ab] and Robert Mokaya *[a]

This work shows how knowledge of any biomass and choice of carbonisation process can offer a generalised route to predictability in the preparation of activated biocarbons. We demonstrate that based on O/C ratio of carbonaceous matter, it is possible to predictably generate biocarbons with suitable porosity, surface area density, volumetric surface area and packing density targeted towards record levels of CO_2 and CH_4 storage capacity. Highly porous carbons with controlled levels of microporosity of up to 97% of the surface area and 92% of the pore volume are generated. The level of synthetic control is such that it enables, on the one hand, exceptional CO_2 storage at 25 °C and low pressure (1.5 and 5.4 mmol g^{-1} at 0.15 and 1 bar, respectively) or moderate pressure (23.7 mmol g^{-1} at 20 bar), indicating superior uptake under both post-combustion and pre-combustion CO_2 capture conditions. The carbons may also be directed towards storing record levels of methane; at 25 °C and 100 bar, volumetric methane uptake of between 309 and 334 cm^3 (STP) cm^{-3} was obtained, which values are considerably higher than all current benchmark materials and, moreover, surpass the United States Department of Energy (US DOE) target of 263 cm^3 (STP) cm^{-3}. Crucially, the carbons also have very attractive working capacity (deliverable methane for 100–5 bar) of 262 cm^3 (STP) cm^{-3}, 234 cm^3 (STP) cm^{-3} (80–5 bar), and 210 cm^3 (STP) cm^{-3} (65–5 bar).

Received 20th July 2022,
Accepted 27th September 2022

DOI: 10.1039/d2ee02322a

rsc.li/ees

Broader context

Activated carbons are a major type of porous material and one of the most widely studied class of solids for use in applications related to sustainable energy provision and environmental remediation. However, current synthesis approaches to activated carbons lack generalised routes *via* which they may be predictably prepared so as to target properties suitable for specific applications. To address this major challenge, this manuscript presents on generalised predictability in the synthesis of biocarbons that goes beyond current synthesis approaches that are based on trial and error. We demonstrate that the amount of fixed carbon and more specifically the ratio of elemental oxygen to elemental carbon (*i.e.* O/C atomic ratio) of biomass-derived carbonaceous matter can be used as a generalised predictor of the nature of porosity generated in an activated carbon. The predictable synthesis enables the preparation of biomass-derived carbons biocarbons) with unique combinations of properties, with respect to porosity, surface area density, volumetric surface area and packing density. The predictable synthesis offers biocarbons with exceptional CO_2 or CH_4 storage; CO_2 uptake of up to 5.4 mmol g^{-1} at 25 °C and 1 bar, and CH_4 of up to 334 cm^3 STP cm^{-3} at 25 °C and 100 bar.

1. Introduction

Growing concerns regarding climate change and related environmental issues have encouraged considerable efforts to control the emission of CO_2, a major greenhouse gas. To reduce the amount of emitted CO_2, there are considerable efforts aimed at carbon capture and storage (CCS) as an intermediate solution. However, the ever increasing global consumption of fossil fuels and rising concerns over the sustainability of oil reserves have stimulated research in alternative energy sources. In this regard, natural gas, with its better environmental sustainability properties compared to oil-based fuels, has been touted as a cleaner alternative energy source. However, methane's volumetric energy density at standard temperature and pressure conditions, being only 0.12% of that of gasoline has limited its practical applications.[1–6] Strategies for increasing the energy density of methane have included liquefaction or compression. However, both are generally viewed as not being viable under ambient temperature and pressure conditions;

[a] *School of Chemistry, University of Nottingham, University Park, Nottingham NG7 2RD, UK. E-mail: r.mokaya@nottingham.ac.uk*
[b] *Department of Chemistry, College of Science, Jouf University, P.O. Box 2014, Sakaka, Saudi Arabia*

† Electronic supplementary information (ESI) available: Two schemes depicting the carbonisation steps, nine additional figures; XRD patterns, TEM images, nitrogen sorption isotherms and pore size distribution curves, comparative gravimetric and volumetric methane uptake isotherms, and five tables; comparative CO_2 and methane uptake. See DOI: https://doi.org/10.1039/d2ee02322a

compressed natural gas needs high-pressure (typically 200–300 bar) conditions that require expensive holding vessels, while liquefied natural gas depends on costly cryogenic cooling techniques. Adsorbed natural gas is, on the other hand, regarded as a promising way forward as it presents advantages with respect to safety, high gravimetric and volumetric energy density and energy efficiency. In this context, it is necessary to find suitable adsorbent materials that are viable for storage of methane and other energy-related gases.[1–7]

Porous carbons, amongst other materials, have been suggested as promising candidates for gas storage applications related to sustainable energy provision where they are explored in relation to other adsorbents, including zeolites and metal–organic frameworks (MOFs).[1–6] Porous carbons, especially activated carbons, can have a competitive edge due to their large-scale availability, low cost, controllable porosity, high thermal and chemical stability, easy preparation, and variable packing density.[7–10] Activated carbons, in particular, can be readily generated from an extensive range of carbon-containing materials.[11–13] Considering the need for sustainability in large-scale gas storage applications of porous carbons, it is worthwhile to prepare them from renewable materials.[14] To this end, biomass-derived porous carbonaceous materials have gained attention due to their ready availability, low cost, renewability, and simple preparation methods.[14–19]

The amount of gas adsorbed and stored on a solid is influenced by the surface area and porosity of the absorbent.[8] In this regard, exploring new trends in the synthesis of tailorable porous materials with large surface area and optimised porosity is one of the long-pursued objectives towards high-performance activated carbons for gas storage applications. The porosity of an activated carbon can be tailored by varying the carbonisation and/or activating processes.[7,10,20] The carbonisation process can dramatically alter the characteristics of both the activatable carbonaceous matter and the final carbon products. Hydrothermal carbonisation (HTC) has long been established as a starting point in transforming biomass into carbon-rich carbonaceous matter that is suitable for activation. The HTC process has the attraction of being relatively simple, only requiring the heating of biomass in water at a typical temperature of 250 °C under autogenous pressure. HTC provides superheated water conditions under which biomass is converted into so-called hydrochar that is amenable to activation.[18,21,22] Air-carbonisation (AC), on the other hand, involves the transformation of biomass to carbonaceous matter at relatively low temperature of *ca.* 400 °C in the presence of air.[7,18,23] Carbonised matter from either process can then be activated, which in this report is *via* a chemical activation step using potassium hydroxide (KOH) as an activating agent. KOH is a preferred activating agent and is widely used to produce carbons with a range of porosity characteristics that can be tailored for enhanced gas adsorption performance.[9,11,18,24,25]

We have recently shown that the carbonisation phase can affect the elemental composition of biomass-derived carbonaceous matter.[7,13,18,23,26] As a consequence, the atomic oxygen/carbon (O/C) ratio is heavily influenced by the nature of the biomass source and the carbonisation process.[7,13,18,23,26] Furthermore, it has also recently been shown that the nature of a carbonaceous precursor has a significant impact on activation behaviour (*i.e.*, susceptibility or resistance to activation) and, consequently, plays a key role in determining the nature of porosity (*e.g.*, micropore/mesopore mix) in the resulting carbons.[7,26] These recent advances are important because the ability to intentionally select or generate targeted biomass-derived carbonaceous precursors can provide activated carbons with predictable and tailored properties for specific applications.

More generally, extensive research findings have demonstrated that biomass-derived activated carbons can show real-world application potential for gas storage.[7,10,13,20,25,27] To this end, biomass-derived activated carbons have been explored for methane storage.[7,28] A practical target for methane storage has recently been set by the US Department of Energy (DOE) at 350 cm^3 (STP) cm^{-3} of volumetric storage capacity and 0.5 g (CH_4) g^{-1} of gravimetric storage capacity at room temperature and pressure of 35–100 bar. It is worth noting that the 350 cm^3 (STP) cm^{-3} target was set at that level based on the crystallographic density of MOFs.[3,4] MOFs have a crystallographic density at least 25% higher than their actual packing density. Hence, this target allows for a 25% reduction in volumetric capacity (to *ca.* 263 cm^3 (STP) cm^{-3}) due to the need to pack MOFs into a storage tank. It is important to note that, in the case of activated carbons, no reduction is anticipated as the volumetric uptake can be obtained using experimentally determined packing density. This means that the target for methane storage in carbons can be taken to be 263 cm^3 (STP) cm^{-3}. An adsorbent's density is key in determining volumetric storage capacity because the adsorbent must be confined in a specific volume (*e.g.* in a tank), and therefore the higher the adsorbent density, the higher the amount of material that can be restricted in a tank and thus the higher the storage capacity.[3,4] To achieve a high packing density, an adsorbent's porosity should arise predominantly from micropores, which may be accompanied by the presence of some small mesopores.

This work demonstrates clear predictability in the synthesis of biomass-derived activated carbons that are intentionally targeted to have properties suitable for CO_2 and CH_4 storage. Clove (*Syzygium aromaticum*) was selected as starting material because it has a relatively low elemental oxygen content. The carbonisation process (AC or HTC) was used along with variation in the activation temperature and the amount of activating agent, to control the textural properties of the resulting activated carbons. The motivation of the study is that cloves, based on their elemental composition and in particular oxygen content and O/C atomic ratio, can be used to predictably generate activated carbons with the appropriate porosity and high packing density that are suited for achieving exceptional levels of CO_2 and CH_4 storage capacity. Although cloves have been used to demonstrate the predictability, the implications are more general and point to the use of either (i) biomass starting material with a low O/C ratio (such as cloves), which yield activateable carbonaceous matter with low O/C ratio or (ii) any biomass that can be transformed into activateable carbonaceous matter with low O/C ratio. In this regard, the cost of producing activated

carbon in a predictable manner (from cloves or any other suitable biomass) should be no more expensive compared to that of already used biomass sources for any commercially available carbons.

2. Experimental section

2.1 Synthesis of biomass-derived activated carbons

Air carbonization. 2 g of cloves were placed in an alumina boat and heated in a horizontal tube furnace to 400 °C under a nitrogen atmosphere at a heating ramp rate of 10 °C min^{-1}. Once at 400 °C, the cloves were briefly (5–10 min) exposed to a flow of air, after which the furnace was left to cool under a nitrogen flow (Scheme S1, ESI†). The resulting carbonaceous matter was designated as air carbonised clove, ACC.

Hydrothermal carbonisation (HTC). 4.6 g of cloves were dispersed in 20 ml of deionised water and placed in a stainless-steel autoclave, heated up to 250 °C, maintained at the target temperature for 2 h, and then cooled to room temperature (Scheme S2, ESI†). The resulting solid product, denoted as hydrochar, was obtained *via* filtration, washed abundantly with deionised water, and dried at 100 °C for 24 h. The resulting hydrochar was designated as HCC – hydrochar from cloves.

Chemical activation. The required amount of KOH was thoroughly mixed with the carbon precursor (ACC or HCC) in an agate mortar at a KOH/carbon precursor ratio of 2 or 4. The resulting mixture was loaded onto an alumina boat, placed inside a tubular furnace, and heated at a ramp rate of 3 °C min^{-1} to 600, 700 or 800 °C under a flow of nitrogen. The furnace was held at the final temperature for 1 h, and then allowed to cool under an atmosphere of nitrogen gas. The resulting activated carbons were washed with 20% HCl at room temperature and then filtered, following which they were washed severally with deionised water until neutral pH was achieved for the filtrate. The carbons were then dried in an oven at 100 °C. The activated carbons was designated as ACC*xT* for air-carbonised carbon-derived samples and HCC*xT* for hydrochar-derived samples, where *x* is the KOH/carbon precursor ratio, and *T* is the activation temperature.

2.2 Material characterisation

Elemental, CHN, analysis was performed on an Exeter Analytical CE-440 Elemental Analyser. A PANalytical X'Pert PRO diffractometer was used to perform powder XRD analysis using a Cu-Kα light source (40 kV, 40 mA) with a step size of 0.02° and 50 s time step. Nitrogen sorption analysis (at −196 °C) with a Micromeritics 3FLEX sorptometer was used for porosity assessment and determination of textural properties. Prior to analysis, the carbon samples were degassed under vacuum at 200 °C for 16 h. The surface area was calculated using the Brunauer–Emmett–Teller (BET) method applied to adsorption data in the relative pressure (P/P_0) range of 0.02–0.22, and pore volume was estimated from the total nitrogen uptake at close to saturation pressure ($P/P_0 \approx 0.99$). The relative pressure range for the determination of surface area was monitored in all cases such that there was a positive *y*-axis intercept from multipoint BET fitting (*i.e.*, $C > 0$) and also that $V_{ads}(1 - p/p_0)$ would rise with P/P_0.[29] The micropore surface area and micropore volume were determined *via t*-plot analysis. The pore size distribution (PSD) was determined using Non-local density functional theory (NL-DFT) applied to nitrogen adsorption data. The determination used SAIEUS software wherein the applied 2D-NLDFT heterogeneous surface kernel allowed adequate consideration of the chemical and energetic heterogeneity of the carbons. The fitting parameter, λ, within the SAIEUS software that controls the PSD's roughness was between 2.5 and 5.0.[30,31] Scanning electron microscopy (SEM) images were recorded using an FEI Quanta200 microscope, operating at a 5 kV accelerating voltage.

2.3 Gas uptake measurements

CO_2 uptake was determined in the pressure range of 0–20 bar at room temperature using a Hiden Isochema Intelligent Gravimetric Analyser (IGA-003). The carbons were outgassed at 240 °C for several hours prior to performing the CO_2 uptake measurements. Methane uptake was determined using a Hiden Isochema XEMIS Analyser. Before the uptake measurements, the carbon samples were degassed at 240 °C under a vacuum for several hours. Methane uptake isotherms were obtained at 25 °C over the pressure range of 0–100 bar.

3. Results and discussion

3.1 Yield and elemental composition of activated carbons

The yields of air-carbonised clove (ACC), clove-derived hydrochar (HCC) and activated carbons are summarised in Tables 1 and 2. The yield of activated carbons was monitored so as to enable a comparison between the air carbonisation route and the conventional HTC route. The yield of air-carbonised cloves (ACC) is similar to clove-derived hydrochar at 35%. However, the yield of ACC-derived activated carbons ranges from 25 to 50%, while that of HCC-derived samples was lower at between 11% and 40%. For any given activation conditions, the yield *via* AC is higher than for HTC, and in some cases is twice as high. It is clear that the air carbonisation route offers higher yields of activated carbons than the conventional HTC route, indicating that air carbonisation generates carbons that are relatively resistant to activation with KOH due to having a lower O/C ratio as confirmed in Tables 1 and 2.[7,18] Similar trends in yield between AC and HTC routes have previously been observed for activated

Table 1 Carbonisation yield and elemental composition of raw clove, air-carbonised clove (ACC) and ACC-derived activated carbons

Sample	Yield [%]	C [%]	H [%]	N [%]	O [%]	O/C[a]
Clove	—	49.7	5.9	0.9	43.5	0.66
ACC	35	66.1	4.3	1.9	27.7	0.31
ACC2600	50	76.5	1.1	0.6	21.8	0.21
ACC2700	47	84.3	0.5	0.3	14.9	0.13
ACC2800	44	87.3	0.2	0.3	12.2	0.11
ACC4600	42	78.4	0.6	0.3	20.7	0.20
ACC4700	37	89.3	0.2	0.3	10.2	0.09
ACC4800	25	90.9	0.2	0.2	8.7	0.07

[a] Atomic ratio.

Table 2 Carbonisation yield and elemental composition of clove, clove hydrochar (HCC) and HCC-derived activated carbons

Sample	Yield [%]	C [%]	H [%]	N [%]	O [%]	O/C[a]
Clove	—	49.7	5.9	0.9	43.5	0.66
HCC	35	62.1	6.3	1.5	30.1	0.36
HCC2600	40	79.0	0.4	0.3	20.3	0.19
HCC2700	37	83.0	0.4	0.4	16.2	0.15
HCC2800	24	86.2	0.1	0.2	13.5	0.12
HCC4600	15	80.9	0.6	0.6	17.9	0.17
HCC4700	12	88.4	0.3	0.2	11.1	0.09
HCC4800	11	92.1	0.2	0.1	7.6	0.06

[a] Atomic ratio.

carbons derived from other biomass sources such as date seed[7] or sawdust.[18] In general, the carbon yield decreases at greater levels of activation (*i.e.*, higher amounts of KOH and/or activation temperature).

The primary aim of the carbonisation process is to enrich the carbon content of the resulting carbonaceous matter. The elemental composition of the raw clove, the carbonized matter (ACC and HCC), and activated carbons is given in Tables 1 and 2. The elemental composition data is an average of at least three determinations. The elemental composition of raw cloves indicates an O/C atomic ratio of 0.66, which is relatively low compared to many other biomass sources for which the ratio is in the range of 0.75–1.0.[7,18] The carbon content increases following the carbonisation step from 49.7 wt% for the raw clove to 66.3 wt% for ACC and 62.1 wt% for HCC, accompanied by a reduction in O content. Air carbonisation results in a reduction in O content from 43.5 wt% (raw clove) to 27.7 wt% for ACC, which is a lower O content compared to 30.1 wt% for HCC. It is noteworthy that the O/C ratio of ACC (0.31) is slightly lower than that of HCC (0.36), although, in general terms, both carbonaceous products have a relatively low ratio.[7,18] The content of H, N and O, on the other hand, gradually reduces at higher levels of activation. Indeed, the O/C ratio for ACC and HCC are amongst the lowest observed for various biomass sources where the O/C ratio is typically in the range of 0.4–1.0.[7,18] It is noteworthy that the elemental composition of ACC and HCC is comparable to that of carbonaceous matter that is known to exhibit resistance to KOH activation, including air-carbonised date seeds,[7] lignin-derived hydrochar,[7] air-carbonised sawdust[18] and so-called CNL1 carbon.[23] In all cases, activation of both ACC and HCC increases the C content, with the rise being generally more significant at higher levels of activation. The low O/C ratio of the ACC and HCC offers an opportunity to predictably target the porosity and packing density of the resulting carbons as described in the following sections. The expectation is that activated carbons derived from ACC and HCC, by virtue of the low O/C ratio, will be dominated by micropores and therefore exhibit both a high surface area density and enhanced packing density.

3.2 Structure and morphology of activated carbons

X-ray diffraction (XRD) was performed to ascertain the nature of the carbons and their purity with respect to the absence of any crystalline inorganic phases. This is important if any inferences are to be made on the link between O/C ratio of precursors with porosity (especially the surface area density) and packing density. Any inferences require that both the precursors (ACC and HCC) and activated carbons be fully carbonaceous with no inorganic matter. The XRD patterns of the raw clove, air-carbonised clove (ACC), clove-derived hydrochar (HCC) and activated carbons are shown in Fig. S1–S3 (ESI†). The XRD pattern of the HCC and ACC show a broad peak at $2\theta = 22^\circ$, which may arise from minor graphitic/turbostratic carbon domains. The XRD patterns for all the carbons are featureless except for low intensity and broad peaks at $2\theta = 22^\circ$ and 44°, which are typically attributed, respectively, to the (002) and (100) diffractions related to graphitic/turbostratic carbon (Fig. S1, ESI†). The low intensity and broad nature of the peaks suggests the lack of planarity of graphitic domains.[18] According to the XRD patterns of the activated carbons (Fig. S2 and S3, ESI†), the amount of KOH has no significant impact on the graphitic/turbostratic nature of the carbons. At any given activation temperature, the XRD patterns indicate a comparable level of graphitic ordering or graphene stacking.[32] Crucially, all the XRD patterns show no sharp peaks, which confirms the absence of any inorganic matter. Thus, according to the XRD patterns, ACC, HCC and the activated carbons are fully carbonaceous.

Cloves have a bulky morphology with a compact surface lacking any conspicuous porous architecture (Fig. S4, ESI†). After air carbonisation, cavities or cracks appear on the external surface of the ACC sample (Fig. S4, ESI†). However, when clove is converted to hydrochar, some of the clove's original morphology appears to be preserved (Fig. S4, ESI†). Conversely, the morphology of activated carbons shows irregularly shaped particles with relatively smooth surfaces and randomly distributed craters and pores (Fig. S5 and S6, ESI†).[14] Such cavities are consistent with generation of porosity *via* gasification processes.[33] It is interesting to note that this morphology is similar to that of most previously reported activated carbons. This is consistent with the fact that it is now well-recognised that activated carbons produced by KOH activation have similar morphology and that the type of precursor material used has little effect on particle shape.

3.3 Porosity and textural properties

The nitrogen sorption isotherms and the pore size distribution (PSD) curves of air-carbonised activated carbons (ACC*xT*) are displayed in Fig. 1 and 2. All the carbons exhibit type I isotherms, which indicates their microporous nature. Although the quantity of nitrogen adsorbed increases with the severity of activation (*i.e.* higher activation temperature), all ACC2*T* carbons (Fig. 1A) show no variation in the shape of the isotherm. All ACC2*T* carbons have a type I isotherm with a sharp adsorption knee wherein virtually all nitrogen sorption occurs at very low relative pressure ($P/P_0 < 0.01$). A sharp knee indicates the presence of a significant proportion of microporosity and the absence of pores larger than the micropore range (up to 20 Å). As shown in Fig. 1B, the porosity of the ACC2*T* carbons is dominated by 5–20 Å pore channels, with all pores being less

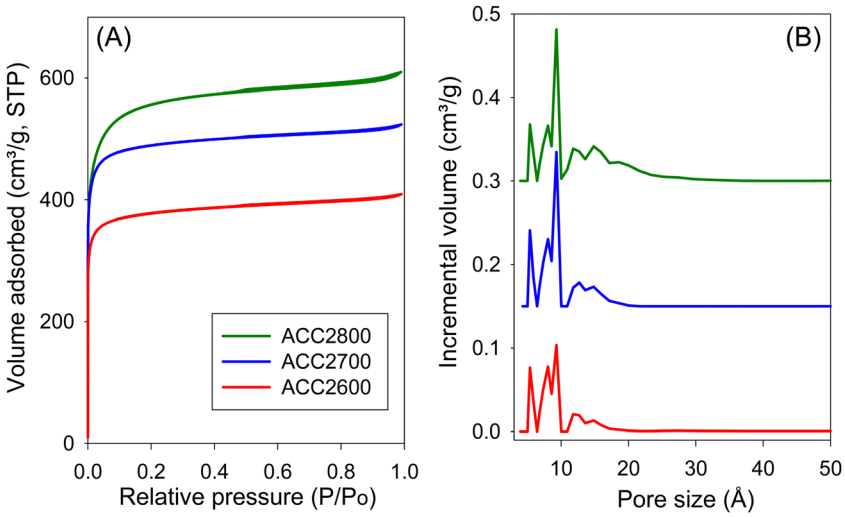

Fig. 1 (A) Nitrogen sorption isotherms and (B) pore size distribution (PSD) curves of activated carbons derived from air-carbonised clove at KOH/ACC ratio of 2.

than 20 Å in diameter. Despite the non-changing shape of the isotherms, the level of porosity, as measured by the amount of nitrogen adsorbed, increases modestly for samples generated at higher activation temperature. The isotherms of ACC4*T* carbons (Fig. 2A) are consistent with a predominantly microporous nature but with a broader knee. Knee broadening, which is greater at higher activation temperature (*i.e.*, more severe activation), indicates presence of larger pores. This is confirmed by the PSD curves in Fig. 2B. Unlike ACC2*T* carbons (Fig. 1B), the ACC4*T* set (Fig. 2B) possess a greater proportion of wider micropores and some small mesopores.

The nitrogen sorption isotherms and PSD curves of hydrochar-derived activated carbons (HCC*xT*) are shown in Fig. 3 and 4. The isotherms of HCC2*T* carbons (Fig. 3A) are type I, with a pronounced sharp adsorption knee at low relative pressure, which is characteristic of essentially microporous materials. The sample activated at 800 °C (HCC2800) exhibits a gentle adsorption knee, implying the presence of supermicropores (pore channels with diameters ranging from 7 to 20 Å) in addition to micropores. This is confirmed by the PSD curves in Fig. 3B; HCC2*T* carbons show few pores larger than 10 Å and no pores wider than 20 Å. Activation at a KOH/HCC ratio of 4 produces a higher proportion of larger pores than activation at a ratio of 2. For example, the isotherms of samples HCC4600 and HCC4700 show a broad adsorption knee, while the sample activated at 800 °C (HCC4800) exhibits a wider adsorption knee with a linear increase in adsorption at relative pressure (P/P_0) up to a of 0.4, indicating the presence of a significant proportion of small mesopores. The PSD curves (Fig. 3B) confirm that HCC4*T* samples have relatively wide PSD but still mainly in the micropore/supermicropore to small mesopore range, with pore channels of up to 34 Å.

The textural properties of both sets of activated carbons are given in Table 3. In the context of all known activated carbons, the surface area and pore volume are moderate to high, depending on the severity of activation. The surface area of ACC2*T* carbons gradually increases from 1500 $m^2\ g^{-1}$ for ACC2600 to 2150 $m^2\ g^{-1}$ for ACC2800, and from 2229 $m^2\ g^{-1}$ for ACC4600 to 3175 $m^2\ g^{-1}$ for ACC4800. This modest increase in surface area for activation at higher temperature is consistent with the resistant to activation nature of ACC.[7] A similar trend is observed for pore volume, which is in the range of 0.63 to 0.94 $cm^3\ g^{-1}$ for ACC2*T* carbons and up to 1.65 $cm^3\ g^{-1}$ for sample ACC4800. It is worth noting that the air-carbonised samples possess a very high proportion of surface area and pore volume arising from micropores, which for ACC2*T* samples is typically *ca.* 96% of the surface area and *ca.* 87% of pore volume, while for ACC4*T* samples it is 81–89% of surface area and 71–79% of pore volume. It is remarkable that the most severely activated sample (ACC4800), still has a proportion of microporosity at 81% (surface area) and 71% (pore volume). For samples prepared *via* hydrothermal carbonisation (HCC*xT*), the surface area of HCC2*T* carbons ranges from 1396 to 2414 $m^2\ g^{-1}$, and the pore volume is in the range of 0.57–1.13 $cm^3\ g^{-1}$, with a very high proportion of micropore surface area of 97%, while micropore pore volume is between 80% and 92%. After the severest activation, sample HCC4800 has the highest surface area and pore volume of 3116 $m^2\ g^{-1}$ and 1.75 $cm^3\ g^{-1}$, respectively, with relatively high microporosity; 70% of surface area and 56% of pore volume.

The surface area and pore volume of air-carbonised ACC2*T* samples are comparable to those of analogous HCC2*T* carbons at any given activation level (*i.e.*, similar temperature and KOH/carbon ratio). However, ACC2*T* have higher levels of microporosity. This trend is also observed for carbons prepared at KOH/precursor ratio of 4, such that although the most severely activated carbons have a comparable total surface area, the air-carbonised sample ACC4800 has a lower pore volume and a significantly higher proportion of microporosity compared to sample HCC4800. This apparent resistance to the formation of larger pores suggests that ACC is relatively more resistant to activation in a manner similar to the recently reported air-carbonised ACSD and ACDS carbons.[7,18] Nevertheless, HCC*xT* carbons also present high levels of microporosity when compared to most other activated carbons,[7,18] which suggests a

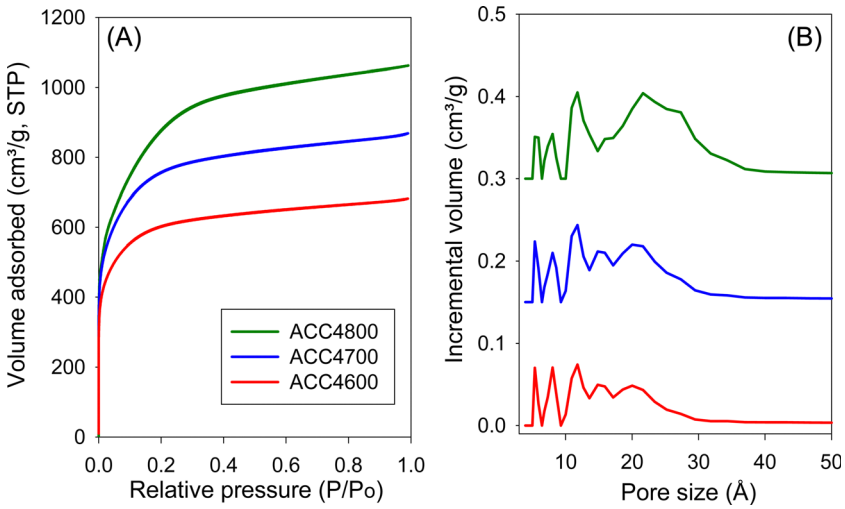

Fig. 2 (A) Nitrogen sorption isotherms and (B) pore size distribution (PSD) curves of carbons derived from air-carbonised clove (ACC) at KOH/ACC ratio of 4.

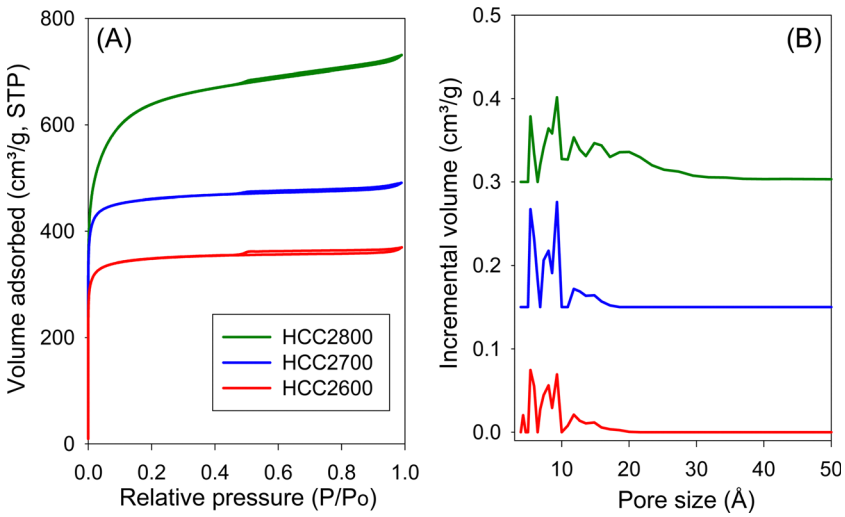

Fig. 3 (A) Nitrogen sorption isotherms and (B) pore size distribution (PSD) curves of activated carbons derived from clove hydrochar (HCC) at KOH/HCC ratio of 2.

significant level of resistance to KOH activation consistent with the relatively low O/C ratio of HCC.

The surface area density (SAD) of the present carbons, which is the ratio of total surface area to total pore volume, is given in Table 3. The SAD of activated carbons is related to the susceptibility or resistance to activation of the carbonaceous precursor from which they are derived. Under any given activation conditions, a high SAD can be well matched with low O/C ratio for the precursor meaning resistance to activation and consequently a tendency to generate micropores rather than mesopores.[7] The O/C ratio can, therefore, be used as a predictor for SAD (*i.e.*, the balance of microporosity and mesoporosity). Moreover, both O/C and SAD may be used to predict the packing density of activated carbons.[7,34,35] Given the low O/C ratio of both ACC and HCC, the expectation was that the resulting activated carbons would have high SAD, which is indeed confirmed in Table 3. The SAD is in the range of 2287–2382 m^2 cm^{-3} for ACC2*T* and 1924–2103 m^2 cm^{-3} for ACC4*T* samples. Given the similarity of the O/C ratio of ACC and HCC, relatively similar values are obtained for hydrochar-derived samples; 2136–2449 m^2 cm^{-3} for HCC2*T* and 1781–2032 m^2 cm^{-3} for HCC4*T* samples. These SAD values are, as predicted, on the higher end compared to that of many other biomass precursors[7] including sawdust hydrochar,[25,36] lignin hydrochar,[37] jujun grass hydrochar[38] and Camelia Japonica hydrochar.[38]

The packing density of porous carbons plays a crucial role in determining the volumetric surface area and volumetric gas uptake, wherein the adsorbing material is filled into a tank with restricted space.[34] In such a scenario, increasing the packing density *via* compaction can improve the volumetric uptake of porous materials. However, such compression is only beneficial

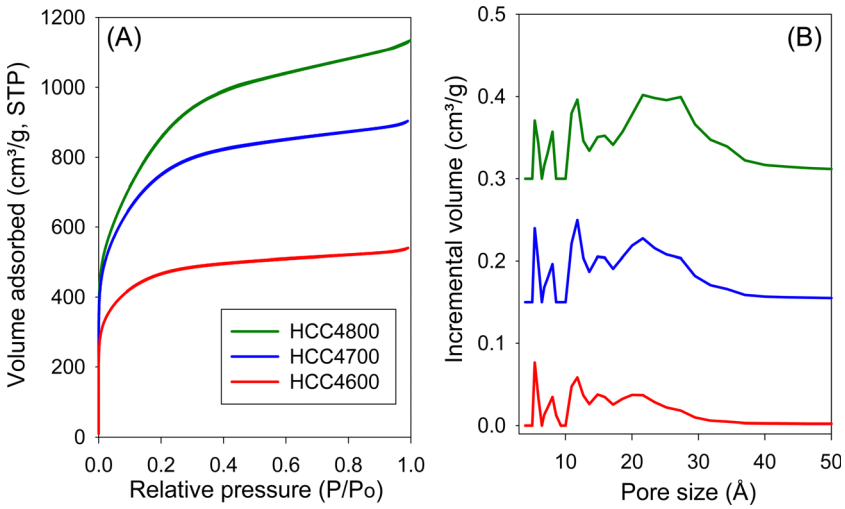

Fig. 4 (A) Nitrogen sorption isotherms and (B) pore size distribution (PSD) curves of activated carbons derived from clove hydrochar (HCC) at KOH/HCC ratio of 4.

Table 3 Textural properties of activated carbons derived from air-carbonised clove (ACC) and clove hydrochar (HCC)

Sample	Surface area ($m^2\ g^{-1}$)	Micropore surface area[a] ($m^2\ g^{-1}$)	Pore volume ($cm^3\ g^{-1}$)	Micropore volume[b] ($cm^3\ g^{-1}$)	Surface area density[c] ($m^2\ cm^{-3}$)	Pore size[d] (Å)
ACC2600	1500	1418 (95%)	0.63	0.55 (87%)	2381	5, 8, 13
ACC2700	1953	1866 (96%)	0.82	0.72 (88%)	2382	5, 9, 13
ACC2800	2150	2019 (94%)	0.94	0.81 (86%)	2287	6, 9, 14
ACC4600	2229	1983 (89%)	1.06	0.84 (79%)	2103	5, 8, 14, 20
ACC4700	2773	2431 (88%)	1.42	1.01 (71%)	1953	5, 8, 14, 21
ACC4800	3175	2568 (81%)	1.65	1.17 (71%)	1924	5, 8, 15, 25
HCC2600	1396	1353 (97%)	0.57	0.52 (91%)	2449	5, 8, 13
HCC2700	1847	1784 (97%)	0.76	0.70 (92%)	2430	6, 8, 13
HCC2800	2414	2163 (90%)	1.13	0.89 (79%)	2136	6, 9, 14, 19
HCC4600	1700	1499 (88%)	0.84	0.65 (77%)	2024	6, 9, 14, 22
HCC4700	2743	2267 (83%)	1.35	1.05 (78%)	2032	6, 9, 15, 24
HCC4800	3116	2190 (70%)	1.75	0.98 (56%)	1781	6, 8, 14, 25

[a] Values in parenthesis are % of surface area from micropores. [b] Values in parenthesis are % of pore volume from micropores. [c] Surface area density is obtained as ratio of total surface area to total pore volume. [d] Pore size maxima from PSD curves.

if it does not compromise the textural properties on which the gravimetric uptake depends.[34] To this end, and with a view of increasing packing density with respect to methane storage, a selection of high surface area HCC-derived carbons (HCC2800, HCC4700 and HCC4800) were compacted at ambient temperature in a 1.3 cm (diameter) die for 10 min at compaction pressure of 370 MPa. The compacted samples were designated as CHCC2800, CHCC4700 and CHCC4800. Only HCC*xT* carbons with the highest surface area (a criteria for good methane storage) were selected for compaction. Given the similarity in textural properties for the high surface area samples in both (HCC*xT* and ACC*xT*) series, the compaction was not duplicated for the latter series of carbons as the expectation was that similar trends would be observed. As shown in Fig. 5 (Fig. S7, ESI†), the nitrogen sorption isotherms and PSD curves of the compacted samples are very similar to those of the non-compacted analogues. This indicates that the compaction does not cause any diminution of porosity or textural properties. As shown in Table 4, in comparison to the data in Table 3 above, there are only minor changes in the textural properties of the carbons after compaction; both surface area and pore volume are largely retained along with the proportion of microporosity, which is enhanced in some cases. As shown in Table 4, despite the retention of their textural properties, the compacted carbons show high packing density of 0.58–0.82 g cm^{-3}.[35]

The surface area density of the compacted samples is within the range of 1792–2146 $m^2\ cm^{-3}$ compared to 1781–2136 $m^2\ cm^{-3}$ for the non-compacted equivalents. Thus SAD does not change on compaction as the overall surface area and pore volume are retained. The volumetric surface area of the compacted carbons, which is defined as surface area x packing density, is also presented in Table 4. The volumetric surface area of porous materials has previously been used as a proxy for gas storage performance, especially for methane.[1,7] The compacted carbons have a volumetric surface area of between 1953 and 1985 $m^2\ cm^{-3}$. The volumetric surface area of these

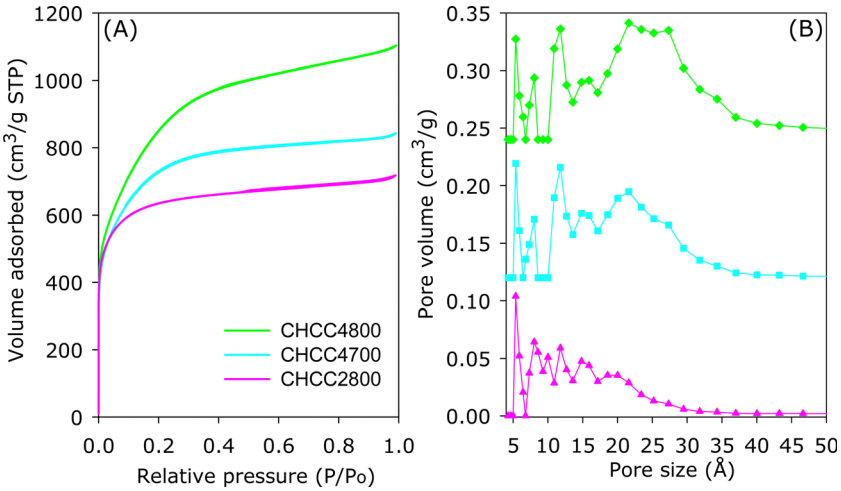

Fig. 5 (A) Nitrogen sorption isotherms and (B) pore size distribution (PSD) curves of compacted carbons derived from hydrochar (HCC).

Table 4 Textural properties of compacted activated carbons derived from clove hydrochar

Sample	Surface area ($m^2\ g^{-1}$)	Micropore surface area[a] ($m^2\ g^{-1}$)	Pore volume ($cm^3\ g^{-1}$)	Micropore volume[b] ($cm^3\ g^{-1}$)	Surf. area density[c] ($m^2\ cm^{-3}$)	Packing density[d] ($g\ cm^{-3}$)	Vol. surface area[e] ($m^2\ cm^{-3}$)
CHCC2800	2382	2170 (91%)	1.11	0.91 (82%)	2146	0.82	1953
CHCC4700	2643	2298 (87%)	1.31	1.02 (78%)	2018	0.75	1985
CHCC4800	3064	2162 (71%)	1.71	1.00 (59%)	1792	0.58	1777

[a] Values in parenthesis are % of surface area from micropores. [b] Values in parenthesis are % of pore volume from micropores. [c] Surface area density is ratio of total surface area to total pore volume. [d] The packing density following compaction at 370 MPa. [e] Volumetric surface area determined as surface area *x* packing density.

carbons is amongst the highest reported for porous materials.[7] Reports of MOFs with higher volumetric surface area exist (*e.g.*, 2060 $m^2\ cm^{-3}$ for NU-1501-Al), but such values are likely to be overestimated as they are computed using crystallographic density rather than actual packing density.[39]

3.4 Gas uptake

3.4.1 CO_2 storage. The CO_2 capture capacity was measured at 25 °C and a pressure range of 0–20 bar. The CO_2 uptake isotherms for ACC*xT* and HCC*xT* carbons are shown in Fig. 6 and 7, respectively, and Table 5 summarises the CO_2 uptake at various pressures (0.15 bar, 1 bar and 20 bar). Generally, the CO_2 uptake isotherms of the ACC2*T* and HCC2*T* carbons prepared at KOH/precursor ratio of 2 approach saturation at 20 bar, whereas those prepared at a ratio of 4 (ACC4*T* and HCC4*T*) are far from saturation, which indicates that they can reach greater storage capacity at higher pressures. As discussed above, the porosity of the ACC2*T* and HCC2*T* carbons is dominated by micropores, while ACC4*T* and HCC4*T* samples have larger micropores and some small mesopores of size up to *ca.* 30 Å. Comparing the porosity data and CO_2 uptake reveals that the CO_2 uptake at low pressures of 0.15 bar and 1 bar is determined by the pore size rather than the total surface area, wherein carbons having narrow micropores show the higher uptake. Narrow micropores have been proven to be more effective at creating stronger interactions between CO_2 molecules and adsorbents than is possible for larger micropores and mesopores.[23] The CO_2 uptake of ACC2*T* samples at 1 bar ranges from 4.5 mmol g^{-1} for ACC2600 to a high of 4.9 mmol g^{-1} for ACC2700. The uptake of ACC2800 is the lowest at 4.2 mmol g^{-1}, which is consistent with the widening of the pore size for this sample (Fig. 3B). The HCC2*T* set of samples show a similar trend; the CO_2 uptake at 1 bar being 4.3 mmol g^{-1} (HCC2600), 5.4 mmol g^{-1} (HCC2700) and 4.2 mmol g^{-1} for HCC2800. Overall, therefore, the ACC2*T* and HCC2*T* set of carbons show very high CO_2 uptake (4.2–5.4 mmol g^{-1}) at 1 bar and 25 °C. On the other hand, the uptake at 20 bar is dependent on surface area meaning that for the ACC2*T* and HCC2*T* set of carbons, it is samples ACC2800 and HCC2800 that have the highest storage capacity (Fig. 6, 7 and Table 5).

At lower pressure (0.15 bar), the CO_2 uptake of ACC2*T* carbons is in the narrow range of 0.9–1.1 mmol g^{-1}, with samples activated at 800 °C having the lowest storage capacity, again consistent with trends in pore size wherein widening of pores results in a reduction of uptake regardless of the variations in the overall surface area and pore volume. The HCC2*T* set of carbons shows a higher uptake of between 0.9 and 1.4 mmol g^{-1}. Generally, the trend matches that of uptake at 1 bar and is clearly related to the microporosity of the carbons.[32] Thus, it is clear that for samples activated at KOH/precursor ratio of 2, the ideal activation temperature for CO_2 uptake at such lower pressures is 700 °C. In particular, the CO_2 uptake for

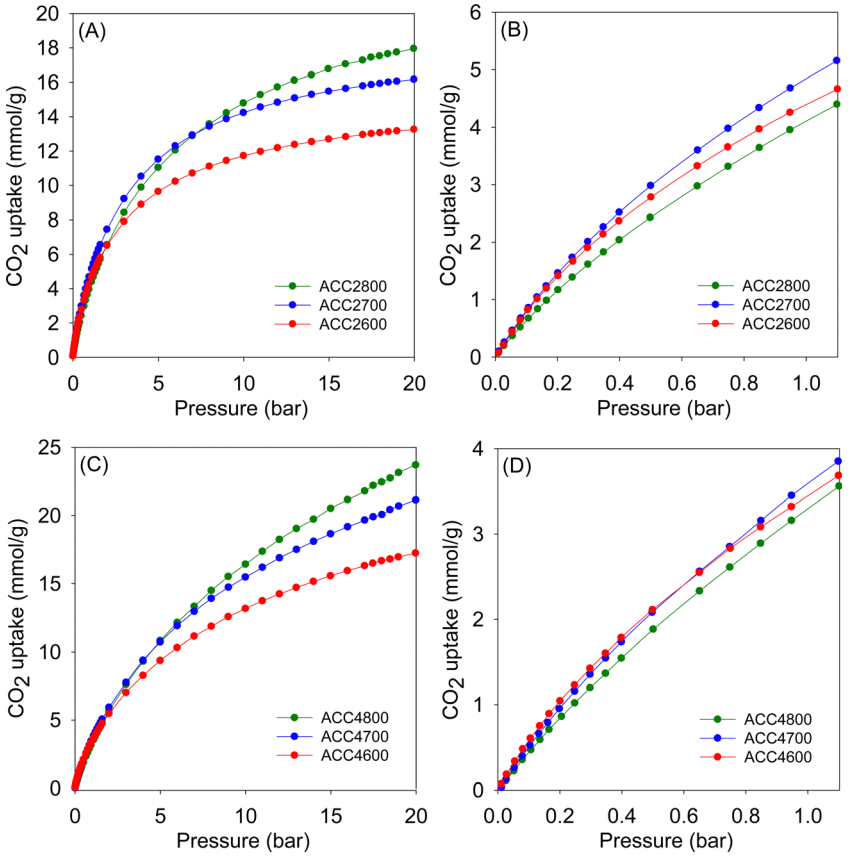

Fig. 6 CO_2 uptake isotherms at 25 °C of activated carbons derived from air-carbonised clove (ACC) prepared at KOH/ACC ratio of 2 (A and B) or 4 (C and D).

sample HCC2700, at 25 °C, of 1.4 and 5.4 mmol g^{-1} at 0.15 and 1 bar, respectively, is at the very top end of what has been observed for all porous carbonaceous materials,[10,13,18,26,27,32,34,37,38,40–42] hence, showing the potential of these carbons as post-combustion CO_2 storage materials. The uptake of HCC2700 is exceptional and one of the highest ever reported for carbons at ambient temperature and pressure, and is due to the sample having both the highest level of microporosity (97% of surface area and 92% of pore volume), and relatively high surface area for such a highly microporous material. Such a porosity combination, which is highly suited for low pressure CO_2 uptake, is unique to the extent that porous carbons rarely show uptake higher than *ca.* 4.8 mmol g^{-1} at 1 bar and 25 °C (Table S1, ESI†).[37,38,40–44] Uptake as high as 5.4 mmol g^{-1} has seldom been observed (Table S1, ESI†) and matches the record values reported to date, namely, 5.8 mmol g^{-1} for compactivated carbons derived from sawdust,[45] 5.67 mmol g^{-1} for fern-derived carbons,[46] and 5.5 mmol g^{-1} for compactivated carbons derived from polypyrrole.[41]

On the other hand, samples having the highest surface area do capture the largest amounts of CO_2 at 20 bar. Consequently, samples ACC4800 and HCC4800, with a surface area of 3175 and 3116 m^2 g^{-1}, respectively, show impressive CO_2 uptake of 23.7 and 23.2 mmol g^{-1} at 20 bar. Rather unusually, these high uptake at 20 bar is alongside attractive uptake at lower pressure of *ca.* 0.7 mmol g^{-1} (0.15 bar) and 3.4 mmol g^{-1} (1 bar). For many previous reports on CO_2 uptake in porous materials, a trend has emerged where materials with a large surface area have high uptake at a pressure of 20 bar or above, but have much lower uptake at a low pressure ($\leq$1 bar). Furthermore, materials characterised by low to moderate surface area and having excellent low-pressure CO_2 uptake generally show low uptake at high pressure. This trend has been ascribed to the fact that the main determinant of CO_2 uptake at low pressure is pore size (and, consequently, the interaction between the gas molecules and pore walls), while the uptake capacity at high pressure is significantly dependent on surface area or space filling. Previous trends are, therefore, somewhat bucked for the present carbons that exhibit superior CO_2 uptake under conditions relevant to both pre-combustion and post-combustion CO_2 capture. Such unique CO_2 uptake is possible for the present carbons because they simultaneously achieve high surface area (and pore volume) and a high level of microporosity. The former ensures good CO_2 uptake at 20 bar while the latter is responsible for attractive low pressure ($<$1 bar) uptake.

Although the present carbons show promise for both pre and post-combustion CO_2 uptake, their microporous nature, especially for ACC2*T* and HCC2*T* samples, is best suited for the latter (*i.e.*, post-combustion CO_2 capture). We therefore further explored the low pressure CO_2 uptake of the ACC2*T* and HCC2*T* series of samples under conditions that mimic post-combustion CO_2 capture from flue gas streams. Table 5 shows the gravimetric

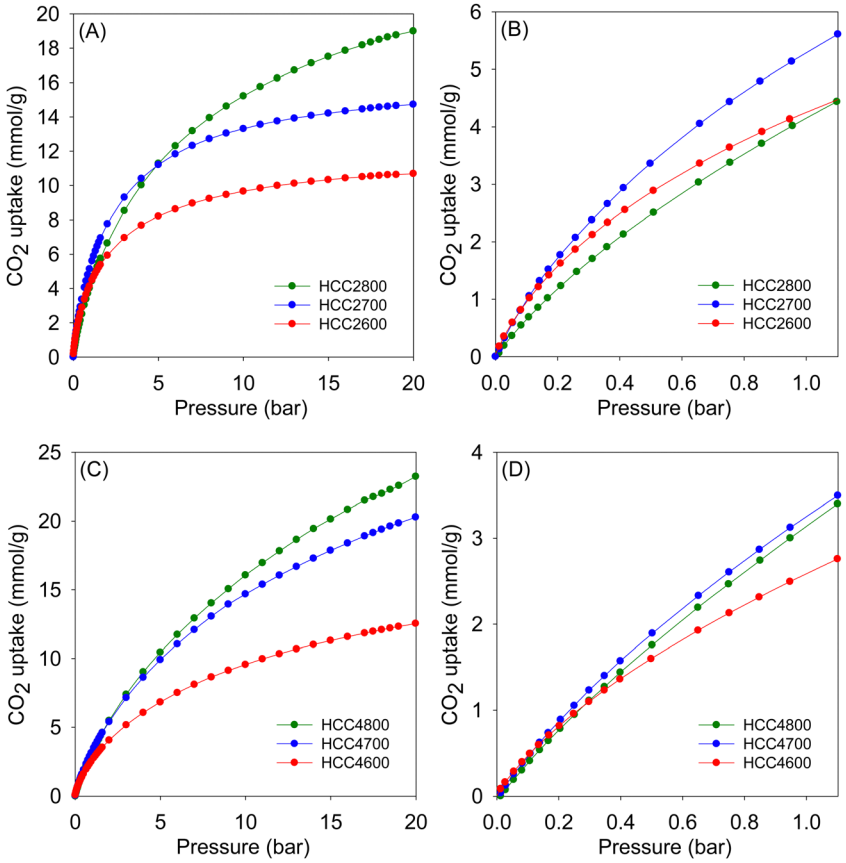

Fig. 7 CO_2 uptake isotherms at 25 °C of activated carbons derived from clove hydrochar (HCC) prepared at KOH/HCC ratio of 2 (A and B) or 4 (C and D).

Table 5 CO_2 uptake of activated carbons derived from air-carbonised clove (ACC) or clove hydrochar (HCC)

Sample	CO_2 uptake (mmol g^{-1}) 0.15 bar	1 bar	20 bar
ACC2600	1.1	4.5	13.3
ACC2700	1.1	4.9	16.2
ACC2800	0.9	4.2	18.0
ACC4600	0.8	3.5	17.2
ACC4700	0.7	3.6	21.1
ACC4800	0.7	3.4	23.7
HCC2600	1.3	4.3	10.7
HCC2700	1.4	5.4	14.7
HCC2800	0.9	4.2	19.0
HCC4600	0.7	2.6	12.5
HCC4700	0.7	3.3	20.3
HCC4800	0.6	3.2	23.2

uptake of the present carbons along with a comparison with benchmark carbons (Table S1, ESI†). To better understand the performance of the present carbons we also determined their volumetric CO_2 uptake. Volumetric uptake is important given that for application in CO_2 capture, the carbons would be packed into a column with limited space (*i.e.*, volume) and therefore the amount of CO_2 stored as a function of the volume occupied by the adsorbing carbon should be optimised. The volumetric uptake takes into account the packing density of the carbons and their gravimetric uptake (Table S2, ESI†). The low-pressure (up to 9 bar) volumetric CO_2 uptake of the ACC2*T* and HCC2*T* samples is impressive (Table S2, ESI†), and is better than or matches that of benchmark carbons[41,45–47] and MOFs.[48–50] In particular, the volumetric uptake of ACC2700 and HCC2700 is exceptional at pressures between 1 and 9 bar and reaches 197 g l^{-1} (100 cm^3 cm^{-3}) at 1 bar, 409 g l^{-1} (208 cm^3 cm^{-3}) at 5 bar, and 482 g l^{-1} (245 cm^3 cm^{-3}) at 9 bar (Table S2, ESI†).

Similar to previous reports on biomass-derived carbons, the present clove-derived carbons exhibit good regeneration and recyclability. Regarding recyclability, of particular interest is the amount of CO_2 that can be sequestered and delivered, *i.e.*, the working capacity, over several cycles of use and reuse. The adsorption and regeneration cycles can be effected *via* pressure swing operations in the form of a pressure swing adsorption (PSA) process or vacuum swing adsorption (VSA) process.[51–53] To work out the working capacity for the present carbons, we considered the following swing adsorption processes; PSA with adsorption at 6 bar and desorption at 1 bar, and VSA with adsorption at 1.5 bar and desorption at 0.05 bar.[53] Cognisant of the nature of flue gas streams from fossil fuel power stations, we determined the working capacity for two scenarios, namely, from a pure CO_2 stream, and from a flue gas stream in which CO_2 constitutes 20% of the gas flow so as to mimic real post-combustion flue gas stream conditions. The gravimetric working capacity is presented in Table 6 along with data for current benchmark activated carbons,[45] high performing MOFs

(Mg-MOF-74 and HKUST-1),[54] and zeolite NaX.[55] For a pure CO_2 stream, the PSA working capacity of the present carbons is between 4.3 and 8.1 mmol g^{-1}, and thus is higher than that of Mg-MOF-74 (3.5 mmol g^{-1}), benchmark carbons (3.4–4.0 mmol g^{-1}) and zeolite NaX (1.6 mmol g^{-1}), and at the high end also surpasses that of HKUST-1 (7.8 mmol g^{-1}). For flue gas conditions, the PSA uptake of the present carbons is between 3.1 and 4.2 mmol g^{-1}, which matches the performance of HKUST-1 (4.5 mmol g^{-1}). The VSA uptake of the present carbons is also very attractive with sample HCC2700 reaching 6.1 mmol g^{-1} and 2.3 mmol g^{-1}, under pure CO_2 and 20% CO_2 conditions, respectively, which when taken together compares favourably with all the other benchmark materials (Table 6).

Furthermore, the volumetric working capacity of the present carbons for both PSA and VSA processes is generally higher than that of the benchmark materials (Table S3, ESI†). For pure CO_2, the PSA volumetric working capacity of the clove-derived carbons is exceptionally high ranging from 185 g l^{-1} (94 cm^3 cm^{-3}) to a high of 257 g l^{-1} (131 cm^3 cm^{-3}) compared to between 142 and 153 g l^{-1} (72–78 cm^3 cm^{-3}) for current benchmark carbons, and is much higher than for Mg-MOF-74 (63 g l^{-1} or 32 cm^3 cm^{-3}) and HKUST-1 (147 g l^{-1} or 75 cm^3 cm^{-3}). Sample HCC2700 has pure CO_2 VSA volumetric working capacity of 223 g l^{-1} (114 cm^3 cm^{-3}) compared to 121 g l^{-1} (62 cm^3 cm^{-3}), 70 g l^{-1} (36 cm^3 cm^{-3}) and 78 g l^{-1} (40 cm^3 cm^{-3}) for HKUST-1, Mg-MOF-74 and zeolite NaX, respectively. Sample HCC2700 also has PSA volumetric working capacity under flue gas conditions of 153 g l^{-1} (78 cm^3 cm^{-3}), which is double that of HKUST-1 and much higher than for zeolite NaX and Mg-MOF-74.

Given that flue gas streams contain majority N_2, it is important to understand the extent to which the present carbons are selective in adsorbing CO_2 over N_2. We therefore determined the selectivity for a representative sample (HCC2700) by comparing the relative uptake at 25 °C and 1 bar of CO_2 and N_2. The comparison (Fig. S8, ESI†) shows that at 1 bar the N_2 uptake is 0.25 mmol g^{-1} compared to CO_2 uptake of 5.4 mmol g^{-1}. This gives an equilibrium CO_2/N_2 adsorption ratio of 22, which is higher than typical ratios of 5–11 for carbon materials.[11,34,42] The selectivity for CO_2 can also be estimated by considering a simulated post-combustion flue gas stream containing *ca.* 15% CO_2 with the remainder as N_2 by comparing the relative uptake of CO_2 at 0.15 bar and N_2 at 0.85 bar. This comparison can give a realistic estimation of selectivity for CO_2 from a scenario that closely mimics real application conditions. Determination of selectivity relies on the ideal adsorbed solution theory (IAST), which is the established model for estimating the relative uptake (or selectivity) by an adsorbent for any two gases in a binary gas mixture.[56] The selectivity (S) for CO_2 can be derived using the IAST model according to the equation; $S = n(CO_2)\,p(N_2)/n(N_2)\,p(CO_2)$, where $n(CO_2)$ is CO_2 uptake at 0.15 bar, $n(N_2)$ is N_2 uptake at 0.85 bar, $p(N_2)$ is 0.85 and $p(CO_2)$ is 0.15. For sample HCC2700 (Fig. S8, ESI†), this determination yields a very high selectivity of 132. The selectivity may also be estimated from the ratio of the initial adsorption rates for CO_2 and N_2, which yields a selectivity factor of 38. The overall picture that emerges is that the clove-derived carbons are highly selective for CO_2 adsorption under post-combustion capture conditions.

As previously postulated[7] and confirmed here, the simultaneously attainment of high surface area and high microporosity, which is responsible for the exceptional CO_2 uptake, is possible due to the resistant to activation nature of the ACC and HCC precursors as indicated by their low O/C ratio. The implications of these findings are that the porosity of activated carbons can be predictably tailored by careful choice of the biomass precursor as guided by its elemental composition and in particular the O/C ratio. In essence, knowledge of the O/C ratio of a carbon precursor can embed predictability in the activation process thus making the synthesis of activated carbons more rational rather than being a random process that is based on trial and error or hit and miss.

Table 6 Gravimetric working capacity for pressure swing adsorption (PSA) and vacuum swing adsorption (VSA) of CO_2 on clove-derived activated carbons compared to benchmark porous materials at *ca.* 25 °C for a pure CO_2 gas stream and a 20% partial CO_2 pressure flue gas stream

	Pure CO_2 uptake[a] (mmol g^{-1})		Flue gas CO_2 uptake[b] (mmol g^{-1})		
Sample	PSA	VSA	PSA	VSA	Ref.
ACC2600	5.7	5.2	3.5	1.8	This work
ACC2700	7.4	5.8	4.0	1.9	This work
ACC2800	7.8	5.1	3.5	1.6	This work
HCC2600	4.3	4.6	3.1	2.0	This work
HCC2700	6.5	6.1	4.2	2.3	This work
HCC2800	8.1	5.2	3.6	1.7	This work
SD2600	3.7	4.6	3.0	2.1	45
SD2600P	3.4	6.0	4.1	2.9	45
SD2650	3.8	4.6	3.1	1.9	45
SD2650P	4.0	5.7	4.0	2.4	45
HKUST-1	7.8	6.4	4.5	1.6	54
Mg-MOF-74	3.5	3.9	2.1	4.1	54
NaX	1.6	2.8	1.8	2.5	55

[a] 1 bar to 6 bar for PSA; 0.05 bar to 1.5 bar for VSA. [b] 0.2 bar to 1.2 bar for PSA; 0.01 bar to 0.3 bar for VSA.

3.4.2 Methane storage. An efficient adsorbent for methane storage should have high surface area and pore volume arising from pore channels of size in the range of 8–15 Å, significant microporosity that is ideally above 85% of the total surface area and/or pore volume, with the rest being small mesopores.[1–7] The present carbons should be ideal candidates to attain high methane storage capacity at moderate to high pressures, particularly given their combination of micro and mesoporosity (Table 4) and high surface area density and volumetric surface area. The methane uptake capacity of the carbons was determined at 25 °C and pressures of between 0 and 100 bar. The methane uptake measurements facilitated direct determination of the excess uptake. The total methane storage capacity was then worked out from the excess data by taking into account the methane density at any given temperature and pressure, and the total pore volume of the activated carbon according to the following equation; $\theta_T = \theta_{Exc} + d_{CH_4} \times V_T$, where θ_T is the total methane uptake, θ_{Exc} is the measured excess methane uptake, d_{CH_4} is the methane gas density (g cm^{-3}) at the prevailing conditions (temperature and pressure) as

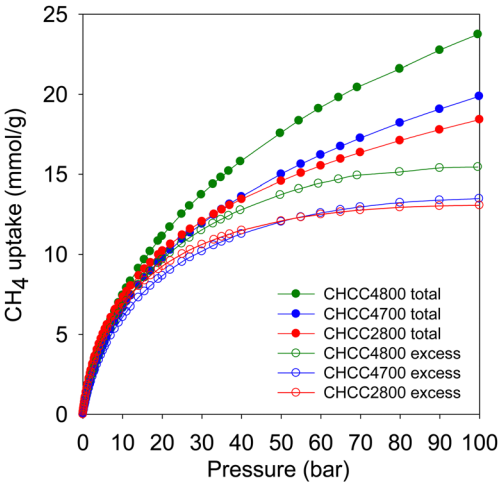

Fig. 8 Excess and total gravimetric methane uptake of compacted activated carbons at 25 °C.

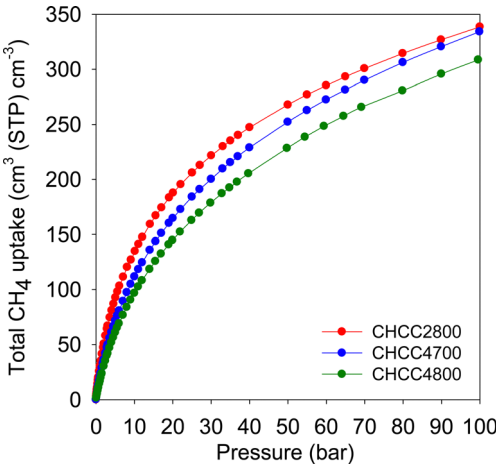

Fig. 9 Total volumetric methane uptake of compacted activated carbons at 25 °C.

obtained from the National Institute of Standards and Technology website (**https://www.nist.gov/**), and V_T is the total pore volume ($cm^3\ g^{-1}$) of the activated carbon.

Fig. 8 shows the excess and total methane uptake isotherms of the CHCC*xT* carbons, and Table 7 summarises the methane storage capacity at 35, 65 and 100 bar. At low pressure, the methane uptake increases sharply with pressure, while a gradual increase occurs in the medium-to-high pressure ranges, and the isotherms are fully reversible. The excess uptake isotherms indicate that the carbons approach saturation at *ca.* 60 bar. The excess uptake follows the trend in surface area, *i.e.*, CHCC2800 < CHCC4700 < CHCC4800. At 35 bar, the excess uptake is in the range of 10.8–12.2 mmol g^{-1}, which increases to between 12.7 and 14.7 mmol g^{-1} at 65 bar, and rises further to 13.1–15.5 mmol g^{-1} at 100 bar. The excess methane uptake compares favourably with data from previous reports.[1–7,39,50,57–63] The excess uptake is within a relatively narrow range, which is consistent with the spread of the porosity of the compacted carbons. The total uptake shows a wider range due to the impact of pore volume in its computation and is between 12.8 and 14.8 mmol g^{-1} at 35 bar, 16.0 and 19.8 mmol g^{-1} at 65 bar, and 18.5 and 23.8 mmol g^{-1} at 100 bar. This values translate to g g^{-1} uptake, respectively at 35, 65 and 100 bar, of 0.21, 0.26 and 0.30 for CHCC2800, 0.21, 0.27 and 0.32 for CHCC4700, and 0.24, 0.32 and 0.38 for CHCC4800. It is noteworthy that, at 100 bar, the g g^{-1} uptake is close to the US DOE target of 0.5 g g^{-1} especially for sample CHCC4800. Such total gravimetric uptake is impressive and comparable to or surpasses that of the best benchmark materials reported to date.[1–7,35,39,50,57–63]

However, the amount of methane adsorbed per unit volume is the most important parameter in terms of the key considerations for methane gas storage applications. The packing density of the adsorbent, along with the gravimetric uptake, play a key role in determining the volumetric uptake. An adsorbent with a high packing density allows more of it to be packed into the restricted storage space (*e.g.* a tank), which effectively drives up the volumetric uptake. The volumetric methane uptake target, set by the US DOE, is 263 cm^3 (STP) cm^{-3} at 25 °C and moderate pressure, *i.e.*, 35–100 bar. Fig. 9 shows the volumetric methane storage isotherms, and Table 8 summarises the uptake at various pressures. Interestingly, the volumetric uptake isotherms reveal no saturation at 100 bar, meaning that the present carbons may store greater amounts of methane at pressures higher than 100 bar. This contrasts with what has been observed for most benchmark MOFs, which saturate at *ca.* 80 bar.[50,64] We attribute this observation to the contribution of the present carbon's mesoporosity to uptake at high pressures, and which also enables efficient adsorption/desorption kinetics.[65] All three compacted carbons exhibit remarkably high volumetric storage capacity (cm^3 (STP) cm^{-3}) being, respectively, 235, 216 and 193 for CHCC2800, CHCC4700 and CHCC4800, at 35 bar. Such uptake at 35 bar is comparable or higher than has previously been reported for any porous

Table 7 Excess and total gravimetric methane uptake for compacted activated carbons

	Gravimetric methane uptake (mmol g^{-1})					
	Excess uptake			Total uptake		
Sample	35 bar	65 bar	100 bar	35 bar	65 bar	100 bar
CHCC2800	11.1	12.7	13.1	12.8	16.0	18.5
CHCC4700	10.8	12.8	13.5	12.8	16.8	20.0
CHCC4800	12.2	14.7	15.5	14.8	19.8	23.8

Table 8 Total volumetric methane uptake and working capacity for compacted activated carbons

	Total volumetric uptake (cm^3 (STP) cm^{-3})			Working capacity[a] (cm^3 (STP) cm^3)		
Sample	35 bar	65 bar	100 bar	35 bar	65 bar	100 bar
CHCC2800	235	293	339	142	200	246
CHCC4700	216	282	334	144	210	262
CHCC4800	193	258	309	132	197	248

[a] The volumetric working capacity is defined as the difference in uptake between the stated pressure (35, 65 or 100 bar) and 5 bar.

carbon;[7,66–75] the best uptake to date is 222 cm^3 (STP) cm^{-3} for an activated carbon (ACDS4700) derived from air-carbonised date seed.[7] More generally, the uptake is comparable to the best MOFs reported so far even though the latter's (MOF's) values, which are calculated using crystallographic density, are known to be overestimated.[1–7,35,39,50,57–63] It is noteworthy that the uptake of CHCC2800 (235 cm^3 (STP) cm^{-3}) surpasses that of the best MOF value, *i.e.*, 224 cm^3 (STP) cm^{-3} for $_{mono}$HKUST-1, where experimental packing density has been used. The monolithic $_{mono}$HKUST-1 has a packing density of 1.06 g cm^{-3} and is claimed to be the current record holder with respect to volumetric methane storage in MOF materials.[1]

At 65 bar, the total methane uptake increases to 293 cm^3 (STP) cm^{-3} for CHCC2800, 282 cm^3 (STP) cm^{-3} for CHCC4700, and 258 cm^3 (STP) cm^{-3} for CHCC4800. There are further increases with pressure such that at 100 bar, the total methane uptake reaches exceptionally high values of 339 cm^3 (STP) cm^{-3} for CHCC2800, 334 cm^3 (STP) cm^{-3} for CHCC4700, and 309 cm^3 (STP) cm^{-3} for CHCC4800. These volumetric uptake values, which are based on experimentally determined packing density, are by some margin the highest ever reported for any porous materials be they carbons or MOFs.[1–7,35,39,50,57–75] For a clearer picture of the performance of the present carbons, Fig. 10 shows how they compare with current benchmark MOFs, including HKUST-1, Ni-MOF-74 and PCN-14.[2–4,76,77] The performance of the current carbons is also compared (Table S4, ESI†) in terms uptake (total volumetric and gravimetric, as g g^{-1}) at 65, 80 and 100 bar to a suite of leading porous materials including Al-soc-MOF-1, MOF-210, NU-1500-Al, NU-1501-Fe and NU-1501-Al, amongst others.[1,3,7,39,48,68,78–81] It is clear from Fig. 10 that the uptake of the present carbons surpasses that of current benchmark carbons and MOFs. This is despite the use of crystallographic density rather than true packing density in calculating values for powder forms of MOFs. It is now accepted that application of crystallographic density overestimates volumetric uptake for MOFs and envisages an impractical scenario where MOFs are packed as single crystals into storage tanks. In practice the actual packing density of MOFs tends to be much lower than crystallographic density with the consequence that the volumetric uptake values for MOFs in Fig. 10 (and Table S4, ESI†) are overestimated by between 25 and 50%. Thus a more realistic comparison is presented is where reductions of 25% are applied to the values of powder MOFs (Fig. S9, ESI†). Comparison with recently reported monolithic forms of MOFs, namely $_{mono}$HKUST-1 and $_{mono}$UiO-66_D,[1,79] removes the ambiguity arising from the use of crystallographic density. It is clear from Fig. 10 (and Fig. S9 and Table S4, ESI†) that the present carbons outperform the monolithic $_{mono}$HKUST-1 and related $_{mono}$UiO-66_D, both of which are claimed to be the current MOF record holders for methane storage at 25 °C and pressure of up to 100 bar.[1,79] Furthermore, the present carbons also have much higher gravimetric uptake, which is almost twice as high compared to $_{mono}$HKUST-1 and $_{mono}$UiO-66_D as shown in Table S4 (ESI†). The exceptional performance of the present carbons, along with their attractive balance between gravimetric and volumetric uptake justifies the targeted synthesis wherein there is control of both the level of the micro/meso-porosity and the packing density *via* careful consideration of the O/C ratio of the biomass-derived precursor.

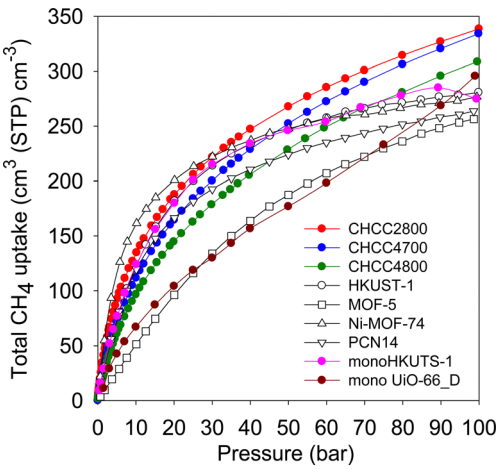

Fig. 10 Total volumetric methane uptake of compacted activated carbons at 25 °C compared to benchmark MOF materials. The uptake of powder MOFs was calculated using crystallographic density.

To fully evaluate the performance of the carbons for methane storage applications, it is crucial to consider the amount (gravimetric and volumetric) of CH_4 that can be delivered, which is commonly referred to as the 'working capacity' or 'deliverable capacity'. In this study, the working capacity is taken as the difference between the adsorbing pressure (35 bar or above) and 5 bar as the desorbing pressure. The volumetric working capacity of the present carbons is given in Table 8 and Table S5 (ESI†) compares their performance to that of a suite of materials. Whilst the present carbons outperform the current benchmark MOF and carbon materials (Table S5, ESI†), the most relevant comparison is with $_{mono}$HKUST-1, which is considered to be the current record holder for volumetric methane storage in porous materials and is claimed to be 50% better than any other MOF.[1] The highest deliverable CH_4 at 100 bar uptake pressure is (262 cm^3 (STP) cm^{-3}) is for sample CHCC4700 compared to (198 cm^3 (STP) cm^{-3}) and (253 cm^3 (STP) cm^{-3}) for $_{mono}$HKUST-1 and $_{mono}$UiO-66_D, respectively.

4. Conclusions

Highly microporous activated carbons were generated from readily-available biomass precursors, cloves (*Syzygium aromaticum*) *via* either hydrothermal carbonisation or flash air-carbonisation followed by chemical activation with KOH. Both carbonisation routes yield carbonaceous matter with low O/C ratio and consequently on activation offer advantages with respect to carbon yield and suitable porosity for exceptional performance in CO_2 and CH_4 storage. The resulting activated carbons have high surface area of up to 3175 m^2 g^{-1} and pore volume of up to 1.85 cm^3 g^{-1}, and depending on activation conditions, present extremely high levels

of microporosity of up to 97% of surface area and 92% of the pore volume. The activated carbons can simultaneously display high CO_2 uptake of 5.4 mmol g^{-1} at 1 bar, and 23.7 mmol g^{-1} at 20 bar and room temperature, which are conditions that mimic post-combustion and pre-combustion CO_2 capture, respectively. Due to their suitably targeted mix of high surface area and pore volume, high packing density, and balance of microporosity-mesoporosity, the activated carbons are also suitable for the storage of methane. Record levels of volumetric methane storage capacity of up to 334 cm^3 STP cm^{-3} were achieved at 100 bar and 25 °C, which is considerably higher than all the benchmark materials and surpass the volumetric CH_4 storage target set by the US DOE target (263 cm^3 (STP) cm^{-3}). Furthermore, they exhibit very high volumetric working capacity of up to 262 cm^3 (STP) cm^{-3} for the pressure range of 100 bar (uptake pressure) to 5 bar (desorption pressure), and 25 °C. This work demonstrates that activated carbons can be predictably synthesised, based on the O/C ratio of biomass-derived activateable carbonaceous matter, in a manner that deliberately targets porosity that is suitable for exceptional CO_2 and CH_4 storage.

Conflicts of interest

There are no conflicts to declare.

Acknowledgements

We thank Jouf University, Kingdom of Saudi Arabia, for funding a PhD studentship for Ibtisam Alali. RM thanks the Royal Society for a Research Grant, and for a Royal Society Wolfson Research Merit Award.

References

1 T. Tian, Z. Zeng, D. Vulpe, M. E. Casco, G. Divitini, P. A. Midgley, J. Silvestre-Albero, J. C. Tan, P. Z. Moghadam and D. Fairen-Jimenez, *Nat. Mater.*, 2018, **17**, 174–179.
2 T. A. Makal, J. R. Li, W. Lu and H. C. Zhou, *Chem. Soc. Rev.*, 2012, **41**, 7761–7779.
3 J. A. Mason, M. Veenstra and J. R. Long, *Chem. Sci.*, 2014, **5**, 32–51.
4 B. Li, H. M. Wen, W. Zhou, J. Q. Xu and B. Chen, *Chem*, 2016, **1**, 557–580.
5 E. Masika and R. Mokaya, *Energy Environ. Sci.*, 2014, **7**, 427–434.
6 Y. Lin, C. Kong, Q. Zhang and L. Chen, *Adv. Energy Mater.*, 2016, **7**, 1601296.
7 A. Altwala and R. Mokaya, *Energy Environ. Sci.*, 2020, **13**, 2967–2978.
8 M. Sevilla and R. Mokaya, *Energy Environ. Sci.*, 2014, **7**, 1250–1280.
9 M. Sevilla, W. Sangchoom, N. Balahmar, A. B. Fuertes and R. Mokaya, *ACS Sustainable Chem. Eng.*, 2016, **4**, 4710–4716.
10 A. M. Aljumialy and R. Mokaya, *Mater. Adv.*, 2020, **1**, 3267–3280.
11 M. Sevilla and A. B. Fuertes, *Energy Environ. Sci.*, 2011, **4**, 1765–1771.
12 M. Sevilla, C. Falco, M. M. Titirici and A. B. Fuertes, *RSC Adv.*, 2012, **2**, 12792–12797.
13 N. Balahmar, A. S. Al-Jumialy and R. Mokaya, *J. Mater. Chem. A*, 2017, **5**, 12330–12339.
14 G. K. Parshetti, S. Chowdhury and R. Balasubramanian, *Fuel*, 2015, **148**, 246–254.
15 O. F. Cruz, J. Silvestre-Albero, M. E. Casco, D. Hotza and C. R. Rambo, *Mater. Chem. Phys.*, 2018, **216**, 42–46.
16 J. Saleem, U. Bin Shahid, M. Hijab, H. Mackey and G. McKay, *Biomass Convers. Bioref.*, 2019, **9**, 775–802.
17 H. Wei, J. Chen, N. Fu, H. Chen, H. Lin and S. Han, *Electrochim. Acta*, 2018, **266**, 161–169.
18 E. A. Hirst, A. Taylor and R. Mokaya, *J. Mater. Chem. A*, 2018, **6**, 12393–12403.
19 G. Singh, K. S. Lakhi, S. Sil, S. V. Bhosale, I. Y. Kim, K. Albahily and A. Vinu, *Carbon N. Y.*, 2019, **148**, 164–186.
20 M. Sevilla, A. S. M. Al-Jumialy, A. B. Fuertes and R. Mokaya, *ACS Appl. Mater. Interfaces*, 2018, **10**, 1623–1633.
21 M. Sevilla and A. B. Fuertes, *Carbon N. Y.*, 2009, **47**, 2281–2289.
22 M. Sevilla, J. A. Maciá-Agulló and A. B. Fuertes, *Biomass Bioenergy*, 2011, **35**, 3152–3159.
23 E. Haffner-Staton, N. Balahmar and R. Mokaya, *J. Mater. Chem. A*, 2016, **4**, 13324–13335.
24 X. L. Zhu, P. Y. Wang, C. Peng, J. Yang and X. Bin Yan, *Chin. Chem. Lett.*, 2014, **25**, 929–932.
25 M. Sevilla, A. B. Fuertes and R. Mokaya, *Energy Environ. Sci.*, 2011, **4**, 1400–1410.
26 N. Balahmar and R. Mokaya, *J. Mater. Chem. A*, 2019, **7**, 17466–17479.
27 A. B. Fuertes and M. Sevilla, *Carbon*, 2015, **94**, 41–52.
28 L. S. Blankenship and R. Mokaya, *Mater. Adv.*, 2022, **3**, 1905–1930.
29 F. Rouquerol, J. Rouquerol and K. Sing, *Adsorption by powders and porous solids: principles, methodology and applications*. 1999, Academic Press, San Diego.
30 P. C. Hansen, *SIAM Rev.*, 1992, **34**, 561–580.
31 P. C. Hansen and D. P. O'Leary, *SIAM J. Sci. Comput.*, 1993, **14**, 1487–1503.
32 A. Altwala and R. Mokaya, *Energy Adv.*, 2022, **1**, 216–224.
33 J. Singh, S. Basu and H. Bhunia, *J. Taiwan Inst. Chem. Eng.*, 2019, **102**, 438–447.
34 B. Adeniran, E. Masika and R. Mokaya, *J. Mater. Chem. A*, 2014, **2**, 14696–14710.
35 D. Lozano-Castelló, D. Cazorla-Amorós, A. Linares-Solano and D. F. Quinn, *Carbon N. Y.*, 2002, **40**, 989–1002.
36 N. Balahmar and R. Mokaya, *J. Mater. Chem. A*, 2019, **7**, 17466–17479.
37 W. Sangchoom and R. Mokaya, *ACS Sustainable Chem. Eng.*, 2015, **3**, 1658–1667.
38 H. M. Coromina, D. A. Walsh and R. Mokaya, *J. Mater. Chem. A*, 2015, **4**, 280–289.
39 Z. Chen, P. Li, R. Anderson, X. Wang, X. Zhang, L. Robison, L. R. Redfern, S. Moribe, T. Islamoglu, D. A. Gómez-Gualdrón, T. Yildirim, J. F. Stoddart and O. K. Farha, *Science*, 2020, **368**, 297–303.

40 M. Sevilla and A. B. Fuertes, *J. Colloid Interface Sci.*, 2012, **366**, 147–154.
41 B. Adeniran and R. Mokaya, *Nano Energy*, 2015, **16**, 173–185.
42 M. Sevilla, P. Valle-Vigõn and A. B. Fuertes, *Adv. Funct. Mater.*, 2011, **21**, 2781–2787.
43 M. Nandi, K. Okada, A. Dutta, A. Bhaumik, J. Maruyama, D. Derksa and H. Uyama, *Chem. Commun.*, 2012, **48**, 10283–10285.
44 G. Sethia and A. Sayari, *Carbon*, 2015, **93**, 68–80.
45 N. Balahmar, A. C. Mitchell and R. Mokaya, *Adv. Energy Mater.*, 2015, **5**, 1500867.
46 J. Serafin, K. Kiełbasa and B. Michalkiewicz, *Chem. Eng. J.*, 2022, **429**, 131751.
47 J. P. Marco-Lozar, M. Kunowsky, F. Suárez-García, J. D. Carruthers and A. Linares-Solano, *Energy Environ. Sci.*, 2012, **5**, 9833–9842.
48 H. Furukawa, N. Ko, Y. B. Go, N. Aratani, S. B. Choi, E. Choi, A. O. Yazaydin, R. Q. Snurr, M. O'Keeffe, J. Kim and O. M. Yaghi, *Science*, 2010, **329**, 424–428.
49 S. R. Caskey, A. G. Wong-Foy and A. J. Matzger, *J. Am. Chem. Soc.*, 2008, **130**, 10870–10871.
50 Y. Peng, V. Krungleviciute, I. Eryazici, J. T. Hupp, O. K. Farha and T. Yildirim, *J. Am. Chem. Soc.*, 2013, **135**, 11887–11894.
51 D. Ko, R. Siriwardane and L. Biegler, *Ind. Eng. Chem. Res.*, 2005, **44**, 8084–8094.
52 E. S. Kikkinides, S. H. Cho and R. T. Yang, *Ind. Eng. Chem. Res.*, 1993, **32**, 2714–2720.
53 L. Wang, Y. Yang, W. Shen, X. Kong, P. Li, J. Yu and A. E. Rodrigues, *Ind. Eng. Chem. Res.*, 2013, **52**, 7947–7955.
54 J. M. Simmons, H. Wu, W. Zhou and T. Yildirim, *Energy Environ. Sci.*, 2011, **4**, 2177–2185.
55 Y. Belmabkhout, G. Pirngruber, E. Jolimaitre and A. Methivier, *Adsorption*, 2007, **13**, 341–349.
56 A. L. Myers and J. M. Prausnitz, *AlChE J.*, 1965, **11**, 121–127.
57 K. V. Kumar, K. Preuss, M. M. Titirici and F. Rodríguez-Reinoso, *Chem. Rev.*, 2017, **117**, 1796–1825.
58 T. A. Rash, A. Gillespie, B. P. Holbrook, L. H. Hiltzik, J. Romanos, Y. C. Soo, S. Sweany and P. Pfeifer, *Fuel*, 2017, **200**, 371–379.
59 D. A. Gómez-Gualdrón, C. E. Wilmer, O. K. Farha, J. T. Hupp and R. Q. Snurr, *J. Phys. Chem. C*, 2014, **118**, 6941–6951.
60 H. Nishihara and T. Kyotani, *Chem. Commun.*, 2018, **54**, 5648–5673.
61 H. Wu, W. Zhou and T. Yildirim, *J. Am. Chem. Soc.*, 2009, **131**, 4995–5000.
62 J. Jiang, H. Furukawa, Y. B. Zhang and O. M. Yaghi, *J. Am. Chem. Soc.*, 2016, **138**, 10244–10251.
63 J. Romanos, S. Sweany, T. Rash, L. Firlej, B. Kuchta, J. Idrobo and P. Pfeifer, *Adsorpt. Sci. Technol.*, 2014, **32**, 681–691.
64 S. Bracco, D. Piga, I. Bassanetti, J. Perego, A. Comotti and P. Sozzani, *J. Mater. Chem. A*, 2017, **5**, 10328–10337.
65 M. E. Casco, M. Martínez-Escandell, K. Kaneko, J. Silvestre-Albero and F. Rodríguez-Reinoso, *Carbon*, 2015, **93**, 11–21.
66 M. E. Casco, M. Martínez-Escandell, E. Gadea-Ramos, K. Kaneko, J. Silvestre-Albero and F. Rodríguez-Reinoso, *Chem. Mater.*, 2015, **27**, 959–964.
67 S. Choi, M. A. Alkhabbaz, Y. Wang, R. M. Othman and M. Choi, *Carbon*, 2019, **141**, 143–153.
68 A. Altwala and R. Mokaya, *J. Mater. Chem. A*, 2022, **10**, 13744–13757.
69 M. E. Casco, F. Rey, J. L. Jordá, S. Rudić, F. Fauth, M. Martínez-Escandell, F. Rodríguez-Reinoso, E. V. Ramos-Fernández and J. Silvestre-Albero, *Chem. Sci.*, 2016, **7**, 3658–3666.
70 A. Kumar, H. P. Veluswamy, R. Kumar and P. Linga, *Appl. Energy*, 2019, **235**, 21–30.
71 D. Lozano-Castelló, D. Cazorla-Amorós and A. Linares-Solano, *Energy Fuels*, 2002, **16**, 1321–1328.
72 Y. He, W. Zhou, T. Yildirim and B. Chen, *Energy Environ. Sci.*, 2013, **6**, 2735–2744.
73 Y. He, W. Zhou, G. Qian and B. Chen, *Chem. Soc. Rev.*, 2014, **43**, 5657–5678.
74 A. Policicchio, R. Filosa, S. Abate, G. Desiderio and E. Colavita, *J. Porous Mater.*, 2017, **24**, 905–922.
75 S. Mirzaei, A. Ahmadpour, A. Shahsavand, H. Rashidi and A. Arami-Niya, *J. Energy Storage*, 2020, **28**, 101251.
76 S. Dutta, A. Bhaumik and K. C.-W. Wu, *Energy Environ. Sci.*, 2014, **7**, 3574–3592.
77 S. Ma, D. Sun, J. M. Simmons, C. D. Collier, D. Yuan and H. C. Zhou, *J. Am. Chem. Soc.*, 2008, **130**, 1012–1016.
78 D. Alezi, Y. Belmabkhout, M. Suyetin, P. M. Bhatt, J. Weseliński, V. Solovyeva, K. Adil, I. Spanopoulos, P. N. Trikalitis, A.-H. Emwas and M. Eddaoudi, *J. Am. Chem. Soc.*, 2015, **137**, 13308–13318.
79 B. M. Connolly, M. Aragones-Anglada, J. Gandara-Loe, N. A. Danaf, D. C. Lamb, J. P. Mehta, D. Vulpe, S. Wuttke, J. Silvestre-Albero, P. Z. Moghadam, A. E. H. Wheatley and D. Fairen-Jimenez, *Nat. Commun.*, 2019, **10**, 2345.
80 J. Jiang, H. Furukawa, Y. B. Zhang and O. M. Yaghi, *J. Am. Chem. Soc.*, 2016, **138**, 10244–10251.
81 B. Wang, X. Zhang, H. Huang, Z. Zhang, T. Yildirim, W. Zhou, S. Xiang and B. Chen, *Nano Res.*, 2021, **14**, 507–511.

